PHYSICAL REVIEW B **93**, 041302(R) (2016)

Transformation of metallic boron into substitutional dopants in graphene on 6*H*-SiC(0001)

J. Sforzini,[1,2] M. Telychko,[3,4] O. Krejčí,[3,4] M. Vondráček,[5] M. Švec,[3] F. C. Bocquet,[1,2,*] and F. S. Tautz[1,2]

[1]*Peter Grünberg Institut (PGI-3), Forschungszentrum Jülich, 52425 Jülich, Germany*

[2]*Jülich Aachen Research Alliance (JARA), Fundamentals of Future Information Technology, 52425 Jülich, Germany*

[3]*Institute of Physics of the Czech Academy of Sciences, Cukrovarnická 10, 16200 Prague, Czech Republic*

[4]*Faculty of Mathematics and Physics, Charles University, V Holešovičkách 2, 18000 Prague, Czech Republic*

[5]*Institute of Physics of the Czech Academy of Sciences, Na Slovance 2, 18221 Prague, Czech Republic*

(Received 5 October 2015; published 19 January 2016)

We investigate the development of the local bonding and chemical state of boron atoms during the growth of B-doped graphene on 6*H*-SiC(0001). Photoemission experiments reveal the presence of two chemical states, namely, boron in the uppermost SiC bilayers and boron substituted in both the graphene and buffer layer lattices. We demonstrate the participation of the dopant in the π electron system of graphene by the presence of the π^* resonance in the near edge x-ray adsorption fine structure (NEXAFS) recorded at the B *K*-edge. The experimental findings are supported by NEXAFS simulations.

DOI: 10.1103/PhysRevB.93.041302

In recent years, graphene has attracted a considerable interest because its physical properties make it suitable for, among others, spintronic devices [1] and transistors [2]. It is well known that covalent and noncovalent modifications of graphene can lead to an enhancement of its magnetic and electrical properties and, consequently, to an improvement of graphene-based devices [3]. For example, substitutional doping, i.e., the replacement of a C atom by a heteroatom in the graphene lattice, is one way to tune the intrinsic properties of graphene. Doped graphene can be used in supercapacitors [4], batteries [5], electrocatalysts [6], and as support for alternative energy devices [7]. While *n*-doped graphene, mostly made through substitutional N doping [8], is extensively studied, *p*-doped graphene, e.g., with B, has been less explored experimentally [9].

In our previous work [10] we demonstrated by scanning tunneling microscopy (STM) that, using a suitable doping procedure, the B dopants are homogeneously distributed in the graphene layer. However, STM experiments do not provide any information on their chemical states in terms of local bonding, their activation, and whether the doping procedure itself influences the substrate underneath the graphene layer. In this Rapid Communication, we present a detailed spectroscopic study of the growth of B-doped graphene on 6*H*-SiC(0001) obtained by depositing B on SiC prior to graphene formation. In contrast to other methods already proposed [11–15], in which either exfoliated graphene or chemical vapor deposition is employed, this preparation ensures a simple routine free of any precursors to achieve high-quality B-doped graphene. We find that the B atoms are incorporated in an identical chemical environment into the graphene layer as well as into the buffer layer, exhibiting the same local structure in both lattices. Moreover, the dopants become part of the π system of graphene and are thus activated. Our experimental results are supported by theoretical calculations. We also show that part of the B diffuses into the SiC bulk.

The experiments were carried out at the Materials Science Beamline at the Elettra Synchrotron. The Si-rich (3×3) surface reconstruction of SiC was prepared by 30 min of annealing at 900 °C under a flux of Si atoms until a sharp and intense low electron energy diffraction (LEED) pattern was obtained. The doping was achieved by depositing B for 1 min from an *e*-beam evaporator keeping the substrate at 900 °C. The B-doped graphene layer was then prepared from the (3×3) reconstruction by annealing slowly for approximately 10 min in 50 °C steps up to 1150 °C. The growth was monitored by LEED, x-ray photoelectron spectroscopy (XPS), and near edge x-ray adsorption fine structure (NEXAFS). The XPS and NEXAFS spectra were recorded with a Specs Phoibos 150 hemispherical electron energy analyzer. The angle between the beamline axis and the analyzer is 60°. We used the following measurement geometries: a grazing incidence geometry (GI), in which the angle between the incident x-ray beam and the surface normal is 60° for XPS and 80° for NEXAFS, and a normal incidence geometry (NI) for NEXAFS only. The XPS spectra were recorded with photon energies of 400, 250 and 150 eV for C 1*s*, B 1*s*, and Si 2*p*, respectively. The binding energies (BEs) were calibrated by measuring the Fermi edge on a tantalum foil. The NEXAFS spectra were acquired at the C and B *K*-edges using KLL Auger yields. For B, the NEXAFS data were normalized to the intensity of the photon flux (measured by a high transmission gold mesh) and subtracted by the background (clean sample). For C, the intensity normalization was not possible because of the mesh contamination and only the background subtraction was applied. STM images were acquired in ultrahigh vacuum and at room temperature using a tungsten tip. In order to confirm the interpretation of the experimental NEXAFS spectra, simulations were performed with the transition potential method [16,17] built within the GPAW code [18,19] and with the spin-polarized general-gradient approximation (GGA) exchange-correlation functional of Perdew, Burke, and Ernzerhof (PBE) [20]. The simulated spectra were broadened by a Lorentzian and a Gaussian of full width at half maximum

*f.bocquet@fz-juelich.de

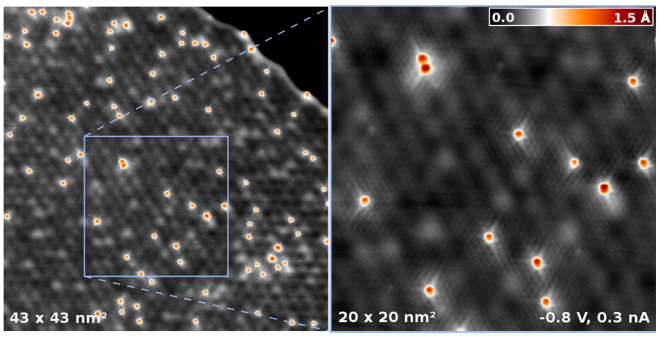

FIG. 1. STM topography images of B-doped bilayer graphene obtained with a bias voltage of −0.8 V and with a tunneling current of 0.3 nA.

(FWHM) 0.1 and 0.5 eV, respectively. The Gaussian FWHM was linearly increased from 0.5 to 10 eV for photon energies from 187 to 207 eV. The structure of freestanding B-doped graphene was optimized with density functional theory (DFT) via the FIREBALL DFT code [21,22].

Figure 1 shows STM images of the doped graphene layer prepared using the method described above. The images are recorded in a bilayer region for better visualization of the B dopants, but we have checked that B atoms show the same incorporation behavior also in single layer graphene. The B atoms, seen as red-orange dots in the image, are present in the graphene layer with a concentration of $(0.13 \pm 0.03)\%$ and are homogeneously distributed. In order to study whether the B atoms are incorporated into the graphene lattice and to find out if the doping also affects the substrate, we turn to photoemission experiments and take advantage of its chemical sensitivity to follow the mechanism of the incorporation of B into the graphene lattice.

Figure 2 shows the XPS spectra of C 1*s* [Fig. 2(a)] and B 1*s* [Fig. 2(c)] core levels at each annealing step during graphene growth, accompanied by the corresponding LEED patterns [Fig. 2(b)]. For the clean Si-rich (3×3) reconstruction a single C 1*s* component at a BE of 282.7 eV is observed. It corresponds to C in the bulk of SiC (C_{SiC}). After depositing the B atoms, a peak at 187.5 eV is detected in the B 1*s* spectra. The annealing step at 950 °C does not affect this peak. Since its BE is found to be the same as the one reported for metallic B [23] and since LEED still presents a sharp (3×3) pattern, we assign this peak to unreacted B present at the surface ($B_{(3\times3)}$). We note in passing that due to previous preparations, a small quantity of $B_{(3\times3)}$ is detectable on the clean (3×3) reconstruction.

After annealing at 1000 °C, a mixture of the Si-rich $(\sqrt{3}\times\sqrt{3})R30^\circ$ and the C-rich $(6\sqrt{3}\times6\sqrt{3})R30^\circ$ (the so-called buffer layer, BL) reconstructions is observed. The distinct band bendings of the two new reconstructions, simultaneously present at this annealing temperature only, broaden the C_{SiC} peak and shift it towards higher BE [24], since now two distinct signals contribute to it: bulk C below the Si-terminated $(\sqrt{3}\times\sqrt{3})R30^\circ$ at 283.2 eV, present only at this annealing step, and second, bulk C below the C-terminated $(6\sqrt{3}\times6\sqrt{3})R30^\circ$ at 284 eV, detected also after annealing to higher temperatures. The formation of the BL, a carbon layer covalently bonded to the topmost Si atoms, stemming from the depletion of Si

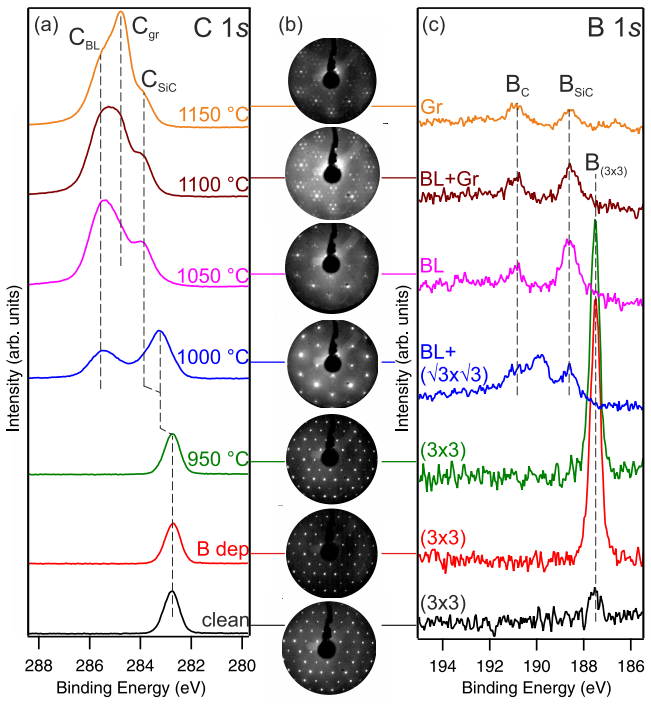

FIG. 2. The XPS spectra of (a) C 1*s* and of (c) B 1*s* measured with a photon energy of 400 and 250 eV, respectively, are shown for each annealing temperature. The corresponding LEED images are displayed in (b).

atoms at high temperature [25] and present only on parts of the surface, produces the peak at 285.3 eV, labeled C_{BL}.

At the same annealing step, the B 1*s* spectrum clearly shows a chemical change, resulting in the appearance of several features. We attribute the central peak at 189.8 eV to an intermediate state related to the $(\sqrt{3}\times\sqrt{3})R30^\circ$ reconstruction, as it appears only at this annealing temperature. The peaks at 188.6 (B_{SiC}) and 190.8 eV (B_C), observed until the final step of graphene formation, must be related to the growth of the C-rich $(6\sqrt{3}\times6\sqrt{3})R30^\circ$ reconstruction, as no band bending induced shift of these peaks is observed between 1000 and 1150 °C. The peak at lower BE, B_{SiC}, detected also in spectra of SiC-B composite powders [26], shows that part of the deposited B in the C-rich region diffuses to the SiC bulk. Our results suggest that this diffusion only occurs at temperatures high enough for the BL to form. The peak at higher BE, B_C, indicates the participation of B in the formation of the BL sp^2/sp^3 lattice.

At higher annealing temperatures (from 1050 to 1150 °C) the BL, in which part of the B is incorporated, transforms into epitaxial graphene, yielding a new component, C_{gr}, at 284.7 eV in the C 1*s* core level spectra [Fig. 2(a)]. This proceeds as a new BL grows underneath. As this process does not affect the B 1*s* chemical environment, no shift of either B_{SiC} or B_C is observed [Fig. 2(c)]. The B_{SiC} intensity decreases with the annealing temperature, which can be explained by a further diffusion of B into the SiC bulk and/or by an attenuation of the signal due to the carbon layers (BL and graphene). In contrast, the B_C intensity is constant, suggesting that the B atoms in the graphene and BL lattices are thermally stable.

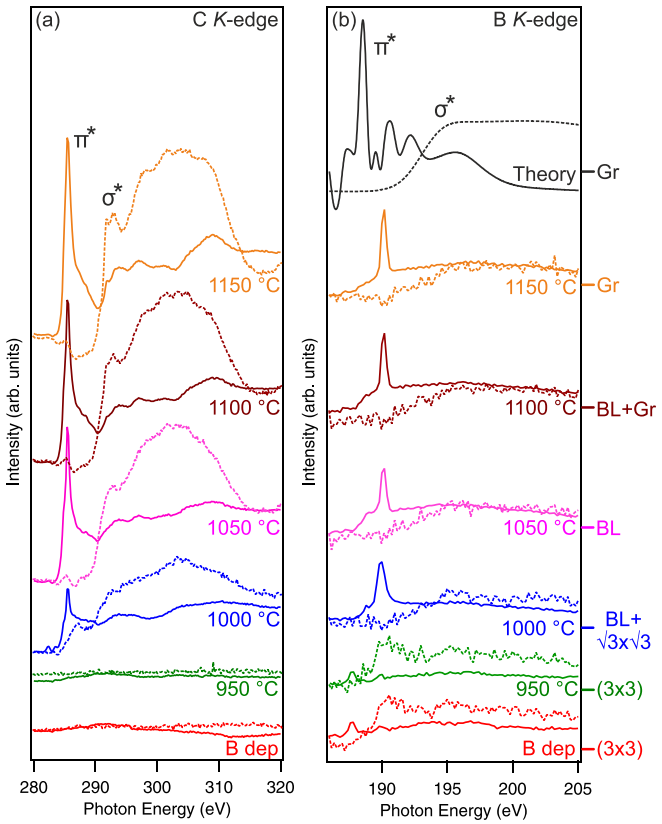

FIG. 3. The NEXAFS difference spectra measured in the GI (continuous line) and the NI geometries (dotted line) of (a) C K-edge and (b) B K-edge are shown for each annealing temperature. The corresponding spectra of the (3×3) reconstruction have been subtracted. The top black curves in (b) present the calculated B K-edge NEXAFS spectra of B-doped freestanding graphene.

Unlike in N-doped graphene [27], there is only one local bonding configuration between the dopant and the host lattice, as evidenced by the single peak B_C at 190.8 eV. Moreover, as no BE shift is observed for B_C between 1050 and 1150 °C, it implies that B has the same chemical environment in the BL and in graphene.

In order to determine this chemical environment, we have carried out NEXAFS experiments, which allow us to distinguish between the sp^2 and sp^3 hybridizations of B. Only in the case of sp^2 hybridization we expect a directionally dependent π^* resonance in our spectra. Figures 3(a) and 3(b) show C K- and B K-edge spectra in grazing (continuous lines) and normal incidence (dotted lines), respectively, from which the corresponding spectra of the clean (3×3) reconstruction have been subtracted. In the B K-edge spectrum no peak is detected for the clean sample in either geometries (not shown). As the (3×3) reconstruction is stable up to 950 °C, no features are detected in the C K-edge difference spectra. However, in the B K-edge difference spectra, a small peak appears in both GI at $h\nu = 187.7$ eV and NI at $h\nu = 190.8$ eV. This peak is related to metallic B on the Si-rich (3×3) reconstruction.

As the C-rich phase starts to evolve above the annealing temperature of 1000 °C, both peaks disappear in the B K-edge spectra, while a new one is observed at $h\nu = 190.1$ eV in GI only. In the corresponding C K-edge spectra the transition from the C 1s initial state to the p_z orbitals (π^* resonance) is detected at $h\nu = 285.5$ eV. As expected, this resonance is quenched in the NI geometry [28], but the transition from the C 1s to the p_{xy} orbitals (σ^* resonance) is visible around $h\nu = 292$ eV in NI [29]. The simultaneous appearance of the carbon π^* transition, accompanied by the formation of B_C and C_{BL} in the XPS spectra of Fig. 2, demonstrates that the peak at $h\nu = 190.1$ eV in the B K-edge spectra is a transition from the B 1s core level to the π system of graphene and the BL. This shows that at least some of the B atoms are indeed incorporated into the host lattices and participate in their π systems. This is confirmed by the expected disappearance of this peak in NI.

In order to support these results, the GI and NI spectra were simulated for B-doped freestanding graphene [Fig. 3(b), top curves]. The behavior of the calculated π^* resonance reproduces our experimental results. According to Ljungberg *et al.* [17], the precision of the Δ Kohn-Sham (ΔKS) approach is within 1 eV. In our case the experimental peaks are shifted by about 1.6 eV towards higher photon energies compared to the calculated ones. This difference can be caused by the effect of the SiC substrate (the calculations being performed on freestanding graphene), which shifts the core levels to higher BE and therefore the corresponding NEXAFS transitions to a higher photon energy.

In summary, we have investigated the chemical state of boron, deposited on the (3×3) reconstruction, during the growth of graphene on 6H-SiC(0001). STM experiments show that the graphene layer is homogeneously decorated by single B atoms. The presence of the π^* transition in the B NEXAFS spectra proves that the B atoms dope the graphene layer by contributing to its π system. Moreover, B is found in a single chemical environment in both the buffer layer and graphene lattices. XPS measurements reveal also that a part of the B atoms diffuse into the upper SiC bilayers. Therefore, we conclude that this preparation is a valid method to obtain high quality B-doped graphene.

F.C.B. acknowledges financial support from the Initiative and Networking Fund of the Helmholtz Association, Postdoc Programme VH-PD-025. This work has been supported by grant agency of the Czech republic, Grant No. 15-07172S. Access to computing and storage facilities owned by parties and projects contributing to the Czech National Grid Infrastructure MetaCentrum, provided under the program "Projects of Large Infrastructure for Research, Development, and Innovations" (LM2010005), is greatly appreciated.

[1] W. Han, R. K. Kawakami, M. Gmitra, and J. Fabian, Graphene spintronics, Nat. Nanotechnol. **9**, 794 (2014).

[2] D. Logoteta, G. Fiori, and G. Iannaccone, Graphene-based lateral heterostructure transistors exhibit better intrinsic performance than graphene-based vertical transistors as post-CMOS devices, Sci. Rep. **4**, 6607 (2014).

[3] D. Kepaptsoglou, T. P. Hardcastle, C. R. Seabourne, U. Bangert, R. Zan, J. A. Amani, H. Hofsäss, R. J. Nicholls, R. M. D.

Brydson, A. J. Scott, and Q. M. Ramasse, Electronic structure modification of ion implanted graphene: The spectroscopic signatures of *p*- and *n*-type doping, ACS Nano **9**, 11398 (2015).

[4] K. Gopalakrishnan, A. Govindaraj, and C. N. R. Rao, Extraordinary supercapacitor performance of heavily nitrogenated graphene oxide obtained by microwave synthesis, J. Mater. Chem. A **1**, 7563 (2013).

[5] Z.-S. Wu, W. Ren, L. Xu, F. Li, and H.-M. Cheng, Doped graphene sheets as anode materials with superhigh rate and large capacity for lithium ion batteries, ACS Nano **5**, 5463 (2011).

[6] C. Zhu and S. Dong, Recent progress in graphene-based nanomaterials as advanced electrocatalysts towards oxygen reduction reaction, Nanoscale **5**, 1753 (2013).

[7] U. Maitra, U. Gupta, M. De, R. Datta, A. Govindaraj, and C. N. R. Rao, Highly effective visible-light-induced H(2) generation by single-layer 1T-MoS(2) and a nanocomposite of few-layer 2H-MoS(2) with heavily nitrogenated graphene, Angew. Chem., Int. Ed. **52**, 13057 (2013).

[8] H. Wang, T. Maiyalagan, and X. Wang, Review on recent progress in nitrogen-doped graphene: Synthesis, characterization, and its potential applications, ACS Catal. **2**, 781 (2012).

[9] D.-A. Yeom, W. Jeon, N. D. K. Tu, S. Y. Yeo, S.-S. Lee, B. J. Sung, H. Chang, J. A. Lim, and H. Kim, High-concentration boron doping of graphene nanoplatelets by simple thermal annealing and their supercapacitive properties, Sci. Rep. **5**, 9817 (2015).

[10] M. Telychko, P. Mutombo, P. Merino, P. Hapala, M. Ondráček, F. C. Bocquet, J. Sforzini, O. Stetsovych, M. Vondráček, P. Jelínek, and M. Švec, Electronic and chemical properties of donor, acceptor centers in graphene, ACS Nano **9**, 9180 (2015).

[11] W. Norimatsu, K. Hirata, Y. Yamamoto, S. Arai, and M. Kusunoki, Epitaxial growth of boron-doped graphene by thermal decomposition of B4C, J. Phys.: Condens. Matter **24**, 314207 (2012).

[12] Z.-H. Sheng, H.-L. Gao, W.-J. Bao, F.-B. Wang, and X.-H. Xia, Synthesis of boron doped graphene for oxygen reduction reaction in fuel cells, J. Mater. Chem. **22**, 390 (2012).

[13] Y. A. Kim, K. Fujisawa, H. Muramatsu, T. Hayashi, M. Endo, T. Fujimori, K. Kaneko, M. Terrones, J. Behrends, A. Eckmann, C. Casiraghi, K. S. Novoselov, R. Saito, and M. S. Dresselhaus, Raman spectroscopy of boron-doped single-layer graphene, ACS Nano **6**, 6293 (2012).

[14] W. Zhao, J. Gebhardt, K. Gotterbarm, O. Höfert, C. Gleichweit, C. Papp, A. Görling, and H.-P. Steinrück, Gold intercalation of boron-doped graphene on Ni(111): XPS and DFT study, J. Phys.: Condens. Matter **25**, 445002 (2013).

[15] Y.-B. Tang, L.-C. Yin, Y. Yang, X.-H. Bo, Y.-L. Cao, H.-E. Wang, W.-J. Zhang, I. Bello, S.-T. Lee, H.-M. Cheng, and C.-S. Lee, Tunable band gaps and *p*-type transport properties of boron-doped graphenes by controllable ion doping using reactive microwave plasma, ACS Nano **6**, 1970 (2012).

[16] L. Triguero, L. G. M. Pettersson, and H. Ågren, Calculations of near-edge x-ray-absorption spectra of gas-phase and chemisorbed molecules by means of density-functional and transition-potential theory, Phys. Rev. B **58**, 8097 (1998).

[17] M. P. Ljungberg, J. J. Mortensen, and L. G. M. Pettersson, An implementation of core level spectroscopies in a real space projector augmented wave density functional theory code, J. Electron Spectrosc. Relat. Phenom. **184**, 427 (2011).

[18] J. J. Mortensen, L. B. Hansen, and K. W. Jacobsen, Real-space grid implementation of the projector augmented wave method, Phys. Rev. B **71**, 035109 (2005).

[19] J. Enkovaara, C. Rostgaard, J. J. Mortensen, J. Chen, M. Duak, L. Ferrighi, J. Gavnholt, C. Glinsvad, V. Haikola, H. A. Hansen, H. H. Kristoffersen, M. Kuisma, A. H. Larsen, L. Lehtovaara, M. Ljungberg, O. Lopez-Acevedo, P. G. Moses, J. Ojanen, T. Olsen, V. Petzold, N. A. Romero, J. Stausholm-Møller, M. Strange, G. A. Tritsaris, M. Vanin, M. Walter, B. Hammer, H. Häkkinen, G. K. H. Madsen, R. M. Nieminen, J. K. Nørskov, M. Puska, T. T. Rantala, J. Schiøtz, K. S. Thygesen, and K. W. Jacobsen, Electronic structure calculations with GPAW: A real-space implementation of the projector augmented-wave method, J. Phys.: Condens. Matter **22**, 253202 (2010).

[20] J. P. Perdew, K. Burke, and M. Ernzerhof, Generalized Gradient Approximation Made Simple, Phys. Rev. Lett. **77**, 3865 (1996).

[21] P. Jelínek, H. Wang, J. P. Lewis, O. F. Sankey, and J. Ortega, Multicenter approach to the exchange-correlation interactions in *ab initio* tight-binding methods, Phys. Rev. B **71**, 235101 (2005).

[22] J. P. Lewis, P. Jelínek, J. Ortega, A. A. Demkov, D. G. Trabada, B. Haycock, H. Wang, G. Adams, J. K. Tomfohr, E. Abad, H. Wang, and D. A. Drabold, Advances and applications in the FIREBALL *ab initio* tight-binding molecular-dynamics formalism, Phys. Status Solidi B **248**, 1989 (2011).

[23] W. E. Moddeman, A. R. Burke, W. C. Bowling, and D. S. Foose, Surface oxides of boron and $B_{12}O_2$ as determined by XPS, Surf. Interface Anal. **14**, 224 (1989).

[24] W. Chen, S. Chen, Z. H. Ni, H. Huang, D. C. Qi, X. Y. Gao, Z. X. Shen, and A. T. S. Wee, Band-bending at the graphene-SiC interfaces: Effect of the substrate, Jpn. J. Appl. Phys. **49**, 01AH05 (2010).

[25] C. Riedl, C. Coletti, and U. Starke, Structural and electronic properties of epitaxial graphene on SiC(0001): A review of growth, characterization, transfer doping and hydrogen intercalation, J. Phys. D: Appl. Phys. **43**, 374009 (2010).

[26] L. Chen, T. Goto, T. Hirai, and T. Amano, State of boron in chemical vapour-deposited SiC-B composite powders, J. Mater. Sci. Lett. **9**, 997 (1990).

[27] M. Telychko, P. Mutombo, M. Ondráček, P. Hapala, F. C. Bocquet, J. Kolorenč, M. Vondráček, P. Jelínek, and M. Švec, Achieving high-quality single-atom nitrogen doping of graphene/SiC(0001) by ion implantation and subsequent thermal stabilization, ACS Nano **8**, 7318 (2014).

[28] J. Stöhr and R. Jaeger, Absorption-edge resonances, core-hole screening, and orientation of chemisorbed molecules: CO, NO, and N_2 on Ni(100), Phys. Rev. B **26**, 4111 (1982).

[29] D. Pacilé, M. Papagno, A. Fraile Rodríguez, M. Grioni, L. Papagno, Ç. Ö. Girit, J. C. Meyer, G. E. Begtrup, and A. Zettl, Near-Edge X-Ray Absorption Fine-Structure Investigation of Graphene, Phys. Rev. Lett. **101**, 066806 (2008).